Interpreting Differences in Radiative Feedbacks from Aerosols Versus Greenhouse Gases

Pietro Salvi[1], Paulo Ceppi[1], and Jonathan M. Gregory[2]

[1]Imperial College London
[2]University of Reading

November 23, 2022

Abstract

Experiments with six CMIP6 models were used to assess the climate feedback parameter for net historical, historical greenhouse gas (GHG) and anthropogenic aerosol forcings. The net radiative feedback is found to be more amplifying (higher effective climate sensitivity) for aerosol than GHG forcing, and hence also more amplifying for net historical (GHG + aerosol) than GHG only. We demonstrate that this difference is consistent with their different latitudinal distributions. Historical aerosol forcing is most pronounced in northern extratropics, where the boundary layer is decoupled from the free troposphere, so the consequent temperature change is confined to low altitude and causes low-level cloud changes. This is caused by change in stability which also affects upper-tropospheric clearsky emission, both affecting shortwave and longwave radiative feedbacks. This response is a feature of extratropical forcing generally, regardless of its sign or hemisphere.

Interpreting Differences in Radiative Feedbacks from Aerosols Versus Greenhouse Gases

Pietro Salvi[1], Paulo Ceppi[1], Jonathan M. Gregory[2,3]

[1]Department of Physics & Grantham Institute, Imperial College London, London, UK
[2]National Centre for Atmospheric Science, University of Reading, Reading, UK
[3]Met Office Hadley Centre, Exeter, UK

Key Points:

- Effective climate sensitivity is larger (feedback more amplifying) for historical anthropogenic aerosol than greenhouse-gas forcing in CMIP6
- The key difference is that greenhouse-gas forcing is global, aerosol mainly extratropical (and aerosol hemispheric contrast unimportant)
- Extratropical forcing causes a shallower temperature response than tropical forcing, hence more positive cloud and lapse rate feedbacks

Corresponding author: Pietro Salvi, `pietro.salvi14@imperial.ac.uk`

Abstract

Experiments with six CMIP6 models were used to assess the climate feedback parameter for net historical, historical greenhouse gas (GHG) and anthropogenic aerosol forcings. The net radiative feedback is found to be more amplifying (higher effective climate sensitivity) for aerosol than GHG forcing, and hence also more amplifying for net historical (GHG + aerosol) than GHG only. We demonstrate that this difference is consistent with their different latitudinal distributions. Historical aerosol forcing is most pronounced in northern extratropics, where the boundary layer is decoupled from the free troposphere, so the consequent temperature change is confined to low altitude and causes low-level cloud changes. This is caused by change in stability which also affects uppertropospheric clearsky emission, both affecting shortwave and longwave radiative feedbacks. This response is a feature of extratropical forcing generally, regardless of its sign or hemisphere.

Plain Language Summary

Understanding how the Earth's surface temperatures change in accordance with the anomalous energy flow into the system due to changes in greenhouse gases (GHGs) or anthropogenic aerosols is vital for predicting future temperature change. New data has made it possible to better calculate how efficiently the planet responds to temperature change (so as to return to energy equilibrium) for historical aerosols and GHGs. We find that the Earth requires greater surface temperature changes under aerosol climate forcing than it does for GHGs in order to balance out incoming and outgoing energy into the Earth system. By comparing with experiments that prescribe energy changes only outside the tropics, we find that the lower efficiency of aerosols is related to their being mainly located away from the equator, unlike GHGs which are generally well mixed throughout the globe. This forcing away from the equator is tied to the vertical distribution of temperature changes, which in turn affects how efficiently surface temperature change leads to balancing the incoming and outgoing energy into the Earth system, leading to different temperature changes for the same global average forcings.

1 Introduction

Global warming due to future emissions of greenhouse gases and other climate forcing agents has been understood in recent years in terms of the energy imbalance that these forcings cause in the Earth system, to which this system responds through changing surface temperatures. The usual interpretive model is $N = F - \alpha T$, where α is the climate feedback parameter, N top-of-atmosphere energy imbalance, T global mean surface temperature change and F effective radiative forcing (Ramaswamy et al., 2001). (Note: we have chosen the sign convention where a positive α implies an increased positive-upwards radiative response for increasing surface temperatures.) Although this is helpful and intuitive as a simple model, there are several complications when using it (Andrews et al., 2015; Knutti & Rugenstein, 2015; Sherwood et al., 2015).

While there are generally confirmed differences in the feedback parameter across models (Andrews et al., 2012; Becker & Wing, 2020; Zelinka et al., 2020), there is not a consensus on whether α depends on the different forcing agents that are relevant to past and future temperature changes. Comparing aerosols and GHGs, the two dominant historical forcing agents (Smith et al., 2020), several studies have found differences in feedbacks (Marvel et al., 2016; Shindell, 2014). Gregory et al. (2020) presented evidence for a difference in α between anthropogenic forcing (GHGs and aerosols) and natural forcing by volcanic aerosol. However, Richardson et al. (2019) did not find significant differences among forcing agents, considering several models in the Precipitation Driver Model Intercomparison Project (PDRMIP) experiments. The focus of this study is the dependence of α on the nature of the forcing agent.

In the recently released data of the Coupled Model Intercomparison Project phase 6 (CMIP6), historical single-forcing experiments across several models have become available for analysis. These new experiments allow us to obtain the effective forcings for different agents, allowing us to accurately calculate the corresponding radiative feedbacks over the historical period. Since previous work has found a dependence on forcing patterns (Andrews et al., 2015; Ceppi & Gregory, 2019; Zhou et al., 2017), which affect the radiation budget via changes in stability and clouds (Andrews et al., 2018), this work considers stability responses to historical greenhouse gases versus historical aerosols and how these correlate with the radiative responses. To do this, we analyse the upward TOA radiative response R, the stability response S as measured by the estimated inversion strength (EIS; Wood & Bretherton, 2006), and the cloud-radiative effect (CRE) measured as the difference in allsky versus clearsky downward fluxes.

2 Methods

Data for several historical forcing experiments was obtained from the ESGF CEDA archive (`esgf-index1.ceda.ac.uk`) for six models: CanESM5, GISS-E2-1-G, HadGEM3-GC31-LL, IPSL-CM6A-LR, MIROC6, and NorESM2-LM. These experiments include a control (piControl) with constant pre-industrial forcing agents, as well as experiments both with coupled atmosphere-ocean models (AOGCMs) and with atmosphere models (AGCMs) given prescribed sea surface conditions, for historical GHGs, aerosols, and all historical forcings together. The different variants which had the required data are detailed in Table S1. Where possible, we chose variants with the same initialisation (i1 variant label), physics and forcing definition as in piControl. We included all realisations that contained all of the required variables, and our results from each experiment of each model are ensemble averages. We calculate multi-model mean (MMM) values from the individual model ensemble averages, with equal weighting for each model.

Prior to analysis, all fields were regridded to a common T42 grid (corresponding to a grid resolution of approximately 2.8° in longitude and latitude), using conservative remapping for radiative fluxes, and bilinear interpolation for other fields. Monthly fields were aggregated into annual averages.

In order to separate out the surface warming (or cooling) driven feedbacks from the forcing and associated rapid adjustments (Hansen et al., 1997; Sherwood et al., 2015), we use the results from the AGCM experiments with fixed sea surface temperatures through the following equation:

$$X_{\mathrm{agent}} = X_{\mathrm{AOGCM}} - X_{\mathrm{AGCM}}, \tag{1}$$

where X represents the variable of interest. Radiative feedbacks and other responses per unit global warming were calculated through linear least-squares regression of the desired variable against global-average surface air temperature.

The confidence intervals for results derived from regressions combine two aspects of uncertainty. The first is the variability among different ensemble members, which we have calculated for each model as the variance across members of the historical experiment. This experiment was chosen since it generally had the most ensemble members, with the assumption that the magnitude of unforced variability is representative of other forcing scenarios. The second is the estimated error in the regression slope of the ensemble-averaged data. The combined error is calculated as the square root of the sum of variances from these two aspects of uncertainty, so they correspond to $\pm 1\sigma$ of the probability distribution.

Two idealised extratropical forcing experiments were run to investigate the impact of forcing localised away from the regions of deep convection on radiative feedbacks and tropospheric stability. These experiments are denoted as nh_extrop and sh_extrop for northern (30°N–90°N) and southern (30°S–90°S) hemisphere forcing respectively. A uniform

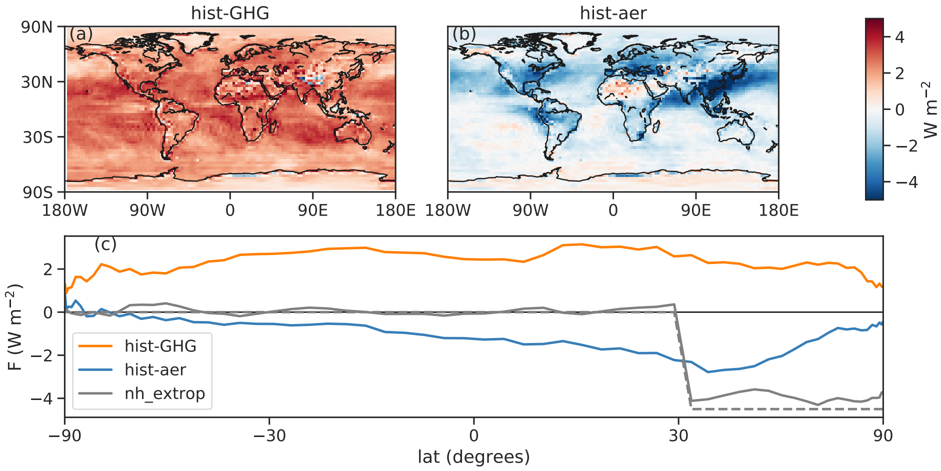

Figure 1. Top-of-atmosphere radiative forcing patterns over years 1995–2014 for hist-GHG (a) and hist-aer (b). The zonal-mean profiles of forcing are shown in (c), where values for hist-GHG (*orange*) and hist-aer (*blue*) are the average effective forcings of the relevant AGCM experiments (piClim-histghg and piClim-histaer, respectively) minus control. For nh_extrop (*grey*) the dashed line shows the prescribed instantaneous forcing whilst the solid line shows the effective forcing calculated from the HadAM3 (atmosphere-only) simulation. Note that the x-axis is scaled by geographical area.

"ghost" radiative forcing of -4.5 W m^{-2} was imposed as an extra term in the surface energy budget in the relevant regions for each experiment. The imposed instantaneous radiative flux values were chosen so that the global average forcing would be comparable to that of hist-aer over years 1995–2014 (around 1.13 W m^{-2}). Though the nh_extrop forcing is zonally uniform unlike the forcing for hist-GHG and hist-aer (Fig. 1a-b), the nh_extrop setup was chosen to capture the skew of the northern extratropical forcing that is seen in hist-aer relative to the more homogeneous hist-GHG (Fig. 1c). The idealised experiments were performed with the Hadley Centre Atmospheric Model version 3 (Pope et al., 2000) in both atmosphere-only (HadAM3) and slab ocean (HadSM3) configurations. The horizontal resolution is 2.5°×3.75°; there are 19 levels in the atmosphere and the slab ocean has a thickness of 50 m. This model is one of the two used by Ceppi and Gregory (2019), and these experiments are the same as their $-\mathrm{UNIF}_{\mathrm{ET}}$ experiment for a single hemisphere at a time, except with a different forcing magnitude.

We also make use of tropical-only forcing experiments in HadSM3 and HadAM3 denoted as "tropical" in later figures. This is the same as the $+\mathrm{UNIF}_{\mathrm{T}}$ experiment in Ceppi and Gregory (2019), which involves a uniform forcing of 7 W m^{-2} over the tropics (30°S-30°N).

3 Investigating radiative feedback differences in terms of stability differences

The radiative feedbacks for historical aerosol and all historical forcings, relative to those from GHGs, are shown in Fig. 2a, for each model analysed and for the MMM. Coloured bars show the allsky net feedback parameter α, whilst markers show the CRE feedback parameter α_{CRE} (minuses) and clearsky feedback parameter α_{CS} (pluses). In all cases, positive numbers mean less amplifying feedbacks, i.e. a relatively larger upward radiative flux perturbation for positive T. The findings here show more amplifying feedbacks for hist-aer than hist-GHG in the MMM. On a model-by-model basis, hist-aer shows either significantly more amplifying or very similar feedbacks to hist-GHG. Neither α_{CS} (correlation of 0.82 with allsky α, Fig. S1b) nor α_{CRE} (correlation of 0.88 with allsky α, Fig. S1d) entirely explains the differences of allsky α for aerosol (or the all historical) compared to GHG forcing, despite correlations here being highly significant ($p<0.001$).

We propose that differences in radiative feedback across forcing agents may be explained in terms of different tropospheric stability responses and their impact on cloud and lapse-rate feedbacks. Fig. 2b shows that hist-aer causes lower stability responses than hist-GHG across all models. A greater increase in stability (as in GHG compared with aerosol) means more warming in the upper troposphere than at the surface, and hence a negative (less amplifying) lapse-rate feedback (Andrews & Webb, 2018; Ceppi & Gregory, 2019). Furthermore, tropospheric stability is a key variable for cloud formation, with higher stability encouraging the formation of low boundary-layer clouds over marine regions (Zhou et al., 2016; Ceppi et al., 2017; Andrews & Webb, 2018; Ceppi & Gregory, 2019). Low clouds have little impact on outgoing longwave radiation due to their temperatures being similar to those at the surface. Since they reflect incoming solar radiation, however, low clouds have an overall positive upwards (cooling) effect on radiation (Hartmann, 1994). Positive forcings that increase stability will thus tend to promote low-level cloudiness and give a positive upwards radiative feedback that opposes the forcing. The feedbacks from increased low cloud, combined with lapse-rate feedbacks, are why we expect a positive correlation between net α and and the stability response S per unit global warming, which we refer to as $\mathrm{d}S/\mathrm{d}T$.

Figure 2c–g supports this inference. Considering all models and experiments together, there is a strong positive correlation between net α and dS/dT (0.72 for the AOGCM experiments, Fig. 2c). Much of the spread in α among this set of models is related to stability, despite our expectation that inter-model differences in climate feedback are dominated by cloud responses to mean SST warming (Ringer et al., 2014). This is still the case when feedbacks are broken down into α_{CS} (Fig. 2e) and, though to a lesser extent, α_{CRE} (Fig. 2g). We interpret the correlation in Fig. 2e as being primarily driven by the linkage between stability and lapse-rate feedbacks (Andrews & Webb, 2018; Ceppi & Gregory, 2019).

By instead considering differences of α in each model of hist-aer and historical from hist-GHG, we remove the model spread, revealing the positive correlation (Fig. 2d) between α and stability change in response to different forcing agents. Although the correlation across models is not very strong (0.65) it is highly significant ($p=0.001$), and the relationship is significant in the MMM according to estimated error bars. The lack of correlation in Fig. 2h, both across models and in the MMM, despite such correlation in Fig. 2f, suggests that the impacts of stability on lapse-rate feedbacks are more robust than the impacts on α_{CRE} for explaining differences in α between historical aerosols and GHGs. This may be because the relationship between S and CRE is not consistently simulated among climate models. Alternatively, it is possible that contrary to the findings of Ceppi and Gregory (2019), global stability changes are not strongly physically linked to CRE in some of the models, and that regional changes in S would be a better explanatory factor.

The historical all-forcing case is dominated by responses to GHGs and aerosols (Smith et al., 2020). Therefore, differences between historical and hist-GHG experiments are due to differences between hist-aer and hist-GHG. Both the feedback parameter (Fig. 2a) and the stability response (Fig. 2b) are greater for historical than for hist-GHG in the MMM. This results from combining hist-GHG and hist-aer responses, given that aerosols and GHGs forcing are of opposite sign (Appendix B in the online supporting information of Gregory and Andrews, 2016). A visual explanation of it can be found in Fig. S2.

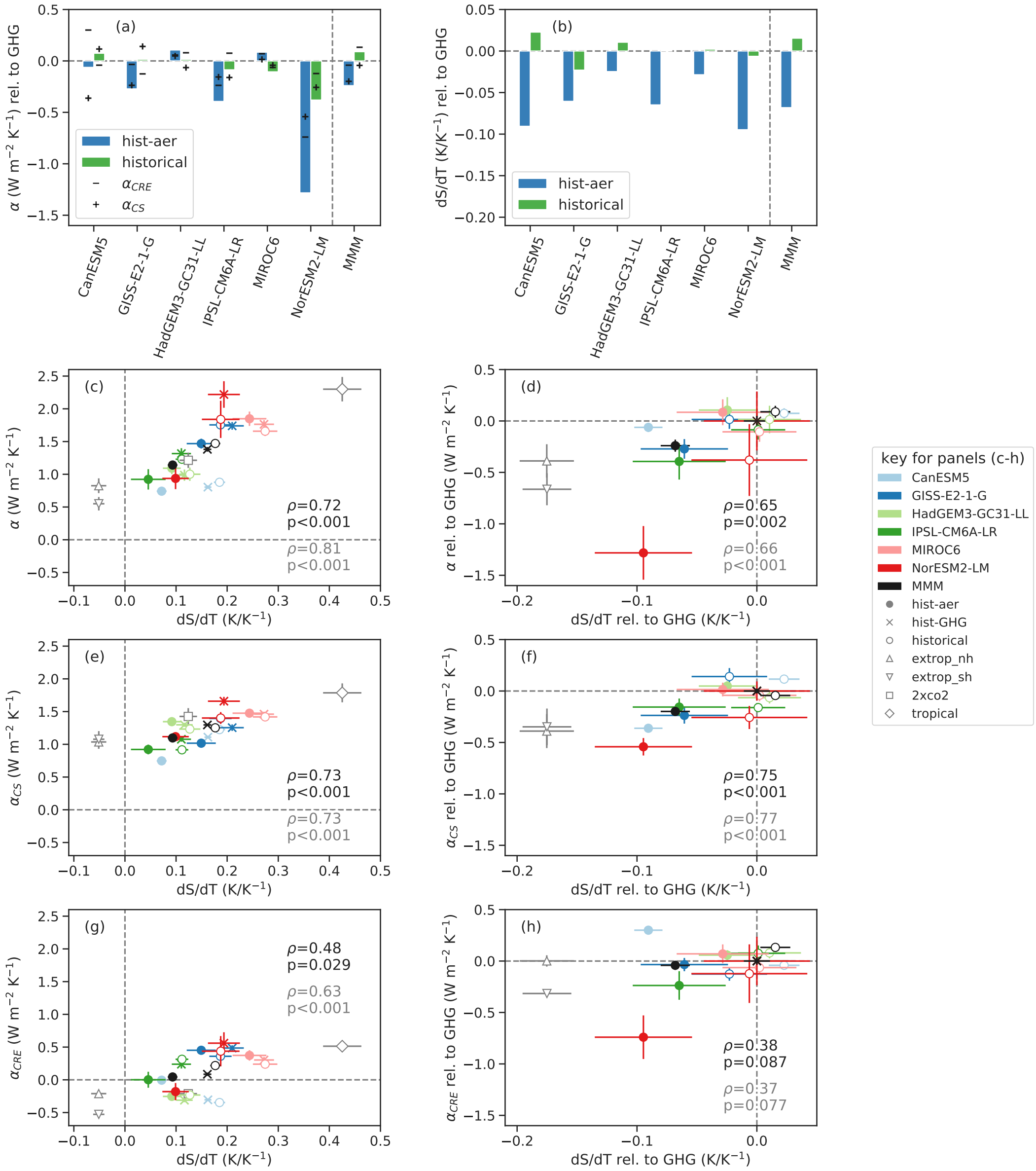

Figure 2. (a) allsky radiative feedback parameter (α, *bars*) alongside CRE (α_{CRE}, *minuses*) and clearsky radiative feedback parameters (α_{CS}, *pluses*) for each model and the multi-model mean, as the difference from hist-GHG values. (b) Difference of $\mathrm{d}S/\mathrm{d}T$ from hist-GHG values. (c,e,g) Net (c) clearsky, (e) CRE, and (g) allsky radiative feedback parameters against net $\mathrm{d}S/\mathrm{d}T$. (d,f,h) as row above, except with values relative to hist-GHG. Confidence intervals in (c-h) denote $\pm$ one standard deviation based off combined regression and ensemble member uncertainties. The Pearson correlation ρ is shown in (c-h), across models and both excluding (*black*) and including (*grey*) the data points from the HadSM3 experiments. The tropical-only forcing experiment is included in (c,e,g), as part of the inter-model trend, but excluded (both in plotting and ρ) in (d,f,h) for clarity and to focus on the HadSM3 experiments that are more similar to hist-aer and hist-GHG. Also shown are p-values for the statistical significance of the correlations.

The results here are in agreement with findings from previous studies of a greater transient climate response (indicative of a less positive α) from aerosols (Marvel et al., 2016) and extratropical forcing (Rose et al., 2014; Rose & Rayborn, 2016; Shindell, 2014) compared to forcing from well-mixed GHGs. By contrast, Richardson et al. (2019) found no significant differences in feedback between two kinds of aerosol (SO_4 and BC) and GHGs, regardless of whether they calculated ERF as in the present paper, or additionally correcting for the impact of land surface temperature adjustments (Andrews et al., 2021). There are several possible explanations for our disagreement, including the following. (1) Despite its statistical significance, the difference we find between feedbacks to aerosol and GHG forcing may be specific to our selection of models, which is smaller than theirs (6, versus 11 in PDRMIP models). (2) Historical aerosol and the 5xSO_4 forcing in PDRMIP night have important differences in feedback, because the contributions of other aerosols than SO_4 are not negligible, although SO_4 forcing is predominant (Myhre et al., 2014). (3) The feedback for a step-like five-fold increase in control SO_4 concentration (as in PDRMIP) may differ from that for the smaller historical SO_4 increases.

4 Explaining stability differences in hist-aer in terms of extratropical forcing

Next, we interpret the distinct radiative and stability responses to aerosols and GHGs in terms of the latitudinal distribution of forcing. Ceppi and Gregory (2019) demonstrated that positive tropical forcing tends to increase global stability per unit global surface warming, while positive extratropical forcing has the opposite impact (and vice versa for negative forcing). To understand why, we recall that the tropics are generally well-coupled to the free troposphere, with the lapse rate closely following a moist adiabat due to moist convection (Flannaghan et al., 2014; Sobel, 2002). Consequently, tropical warming has a relatively large impact on free-tropospheric temperature. Mixing by atmospheric motions propagates the warming signal to the extratropical free troposphere, stabilising the atmosphere there (Fig. 3d). Conversely, positive forcing in the extratropics is expected to decrease stability, since surface temperature in the extratropics is more weakly coupled to the free troposphere. The effects of extratropical surface forcing tend to be more confined near to the surface, and since this forcing acts on a region that is (on average) climatologically stable, the stability response is similar to that found for warming in other stable regions such as in the tropical South-East Pacific (Andrews & Webb, 2018). This effect can be seen by comparing air temperature changes in the hist-aer and hist-GHG cases (Fig. 3e). Note that aerosol forcing is *negative* and causes a surface *cooling*, but the patterns in Fig. 3 are normalised by regression against global mean surface temperature change, and the sign of $\mathrm{d}S/\mathrm{d}T$ is unaffected.

This reasoning could explain why the hist-aer case gives a less positive stability response per unit surface warming than the hist-GHG case. The skew of forcing towards the extratropics in the hist-aer case (blue line in Fig. 1c) means that a relatively larger fraction of the surface temperature response is in vertically decoupled regions, leading to the smaller $\mathrm{d}S/\mathrm{d}T$ than in hist-GHG. In support of this hypothesis, we note that the pattern of tropospheric temperature change in the HadSM3 nh_extrop experiment compared to the 2xco2 experiment (Fig. 3g) is similar to the difference between hist-aer and hist-GHG (Fig. 3e). The pattern from tropical-only forcing (Fig. 3d) shows the propagation of warming to both the tropical and extratropical free tropospheres in accordance with an increase to stability as seen in Fig. 2c–g. Fig. 2e shows that $\mathrm{d}S/\mathrm{d}T$ is negative for both nh_extrop and sh_extrop, whereas it is positive in nearly every historical forcing experiment. This difference is probably related to the absence of tropical forcing in the idealised cases. That the negative $\mathrm{d}S/\mathrm{d}T$ occurs for forcing in both hemispheres suggests that the essential characteristic is that the forcing is extratropical, rather than hemispheric. The historical all-forcing case shows the opposite pattern to hist-aer when com-

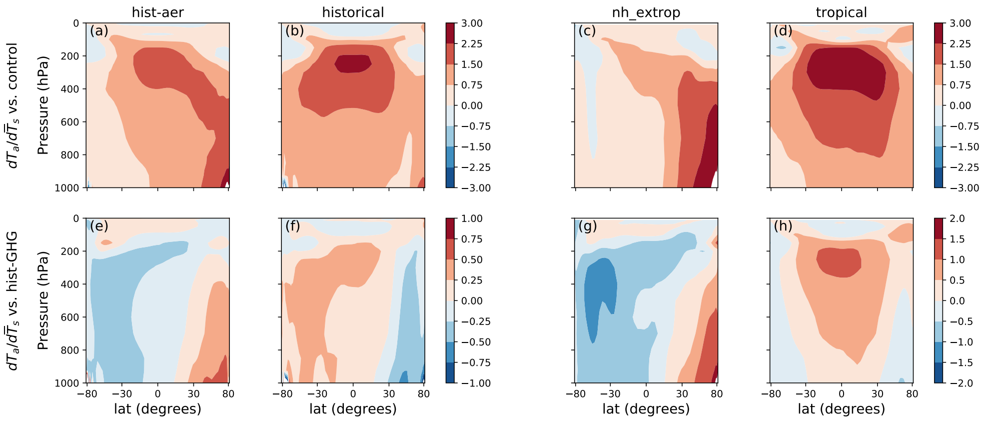

Figure 3. MMM zonal-mean profiles of local air temperature regressed onto global surface air temperature. Values shown are absolute (a–b), and relative to hist-GHG (e–f). Also shown are the results from the HadSM3 NH extratropical forcing (c) and tropical-only forcing (d), and these relative to the HadSM3 2xco2 experiment (g–h). Note that the x-axis is scaled by geographical area.

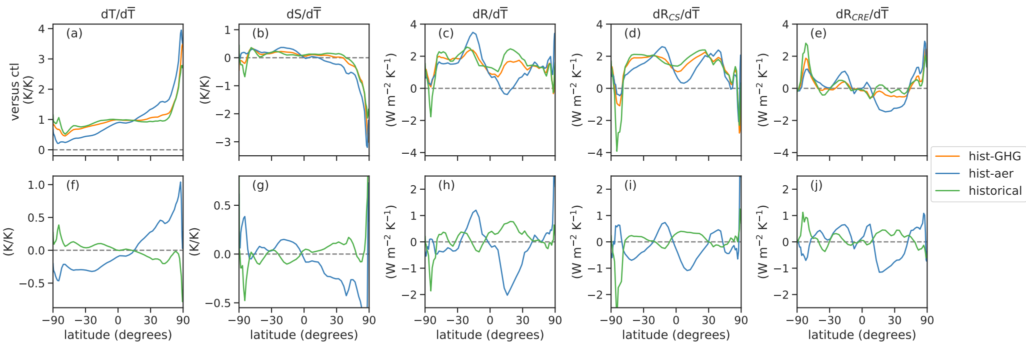

Figure 4. MMM zonal-mean values regressed onto global surface air temperature for the historical cases (*top* row) and differenced relative to hist-GHG (*bottom* row) in terms of (a,f) temperature, (b,g) estimated inversion strength, (c,h) net upwards radiative response, (d,i) upwards radiative response in clearsky and (e,j) upwards radiative response from CRE. Note that the x-axis is scaled by geographical area.

pared to hist-GHG (Fig. 3e–f), indicating that aerosol has a similar effect on stability whether applied independently or jointly with GHGs.

To corroborate this reasoning, we consider the MMM zonal means of feedbacks and climate responses in Fig. 4. There is less meridional contrast in response to hist-GHG than hist-aer (top row). Subtracting the responses from hist-GHG (bottom row), we see a positive NH temperature response per unit global warming in hist-aer relative to hist-GHG, and the opposite in the SH. This anti-correlates with the stability response per unit surface warming, which in turn correlates (in low latitudes) with the radiative response. The radiative response is then finally well explained, in terms of pattern, by the combination of clearsky and CRE feedbacks.

Just as the global average feedbacks for the historical case are more positive than those for hist-GHG, the zonal-mean curves for hist-GHG generally lie between those for the all historical and hist-aer cases (top row of Fig. 4), again consistent with the expected effect of aerosol. Likewise, the difference between historical and hist-GHG responses (bottom row of Fig. 4) can be interpreted as representing the effect of aerosol, but with the sign reversed (see Appendix A in the Supporting Information).

5 Summary and Conclusions

Our analysis of AOGCM historical experiments from CMIP6 (including new experiments which allow forcing to be diagnosed) reveals that climate feedback is more strongly amplifying (greater climate sensitivity) in response to anthropogenic aerosol forcing than greenhouse-gas (GHG) forcing. This difference is shown and is statistically significant in the MMM, though only six AOGCMs have so far provided the required historical experiments and variables for this analysis, so it would be useful to repeat it with more. Our finding is consistent with those from past studies that also found greater climate sensitivity to aerosol than GHGs (Marvel et al., 2016; Shindell, 2014), but appears inconsistent with the recent study of Richardson et al. (2019). Further work is needed to explain the disagreement, which may relate to differences in the details of the prescribed aerosol forcing (e.g. SO_4 only or a mixture of type of aerosol, historical concentration changes or the fivefold increase prescribed by Richardson et al.).

Furthermore, we find that the difference in (positive-stable) net top-of-atmosphere radiative feedback parameter for aerosol and GHG forcing is positively correlated across AOGCMs with a difference in the response of tropospheric stability to the two kinds of forcing. We propose that the difference arises from the different latitudinal distributions of the forcing. An idealised slab model experiment with uniform surface forcing confined to the Northern extratropics qualitatively reproduces the near-surface extratropical temperature change that differentiates the historical aerosol experiment from the historical GHG experiment. The shallower extratropical temperature change in the former is explained by the lower proportion of forcing in the tropics, where the surface is relatively strongly coupled to the free troposphere by deep convection (Flannaghan et al., 2014; Sobel, 2002), compared to the higher proportion of forcing in the extratropics, where the coupling is weaker and the effect of forcing more confined to the surface.

Thus a positive extratropical forcing causes a near-surface warming, which reduces tropospheric stability, whereas a positive tropical forcing has less effect on stability. A reduction in stability tends to reduce low-level cloudiness, which gives an anomalously positive shortwave feedback on warming, whilst it also induces an anomalously positive longwave lapse-rate feedback. In this way, the latitude of forcing is linked to the radiative feedback it produces. Historical aerosol forcing is negative, so the signs of temperature and stability change are reversed, but the feedback parameter, sensitivity of stability (change per unit warming), and hence the correlation with the feedback parameter have the same sign for either sign of forcing: extratropical forcing tends to give higher climate sensitivity. This link accords with previous works that have highlighted the impact of forcing patterns on radiative feedbacks (Ceppi & Gregory, 2019; Rose et al., 2014; Rose & Rayborn, 2016).

Historical climate change is dominated by GHG forcing. Hence the net feedback simulated in the historical experiments with all forcings is nearer to that for GHG than for anthropogenic aerosol. The effective climate sensitivity for historical forcing is slightly *smaller* than for historical GHG forcing (the magnitude of α is larger), because of included historical aerosol forcing, for which climate sensitivity is *larger*, but the sign is opposite. We find also that some of the spread across AOGCMs in the climate sensitivity to GHG forcing is also correlated with the response of tropospheric stability to forcing; this aspect is intriguing and requires further investigation.

Acknowledgments

PS was supported by the Department of Physics and the Grantham Institute of Imperial College London. PC was supported by an Imperial College Research Fellowship and NERC grants NE/T006250/1 and NE/T007788/1. JMG was supported by the European Research Council under the European Union's Horizon 2020 research and innovation programme (grant agreement No 786427, project "Couplet"). This work used JASMIN, the UK collaborative data analysis facility and the ARCHER UK National Supercomputing Service. The data that support the findings of this study are available online. The data from CMIP6 experiments can be found on the ESGF CEDA node available at `esgf-index1.ceda.ac.uk`. The data from the HadSM3 and HadAM3 experiments can be found at
`https://doi.org/10.6084/m9.figshare.17197748` and
`https://doi.org/10.6084/m9.figshare.17182907`.

References

Andrews, T., Gregory, J. M., Paynter, D., Silvers, L. G., Zhou, C., Mauritsen, T., ... Titchner, H. (2018). Accounting for Changing Temperature Patterns Increases Historical Estimates of Climate Sensitivity. *Geophysical Research Letters*, *45*(16), 8490–8499. Retrieved 2019-07-15, from `https://agupubs.onlinelibrary.wiley.com/doi/abs/10.1029/2018GL078887` doi: 10.1029/2018GL078887

Andrews, T., Gregory, J. M., & Webb, M. J. (2015, February). The Dependence of Radiative Forcing and Feedback on Evolving Patterns of Surface Temperature Change in Climate Models. *Journal of Climate*, *28*(4), 1630–1648. Retrieved 2021-12-09, from `https://journals.ametsoc.org/view/journals/clim/28/4/jcli-d-14-00545.1.xml` (Publisher: American Meteorological Society Section: Journal of Climate) doi: 10.1175/JCLI-D-14-00545.1

Andrews, T., Gregory, J. M., Webb, M. J., & Taylor, K. E. (2012). Forcing, feedbacks and climate sensitivity in CMIP5 coupled atmosphere-ocean climate models. *Geophysical Research Letters*, *39*(9). Retrieved 2019-07-23, from `https://agupubs.onlinelibrary.wiley.com/doi/abs/10.1029/2012GL051607` doi: 10.1029/2012GL051607

Andrews, T., Smith, C. J., Myhre, G., Forster, P. M., Chadwick, R., & Ackerley, D. (2021). Effective Radiative Forcing in a GCM With Fixed Surface Temperatures. *Journal of Geophysical Research: Atmospheres*, *126*(4), e2020JD033880. Retrieved 2021-10-29, from `https://onlinelibrary.wiley.com/doi/abs/10.1029/2020JD033880` (_eprint: https://onlinelibrary.wiley.com/doi/pdf/10.1029/2020JD033880) doi: 10.1029/2020JD033880

Andrews, T., & Webb, M. J. (2018, January). The Dependence of Global Cloud and Lapse Rate Feedbacks on the Spatial Structure of Tropical Pacific Warming. *Journal of Climate*, *31*(2), 641–654. Retrieved 2021-10-12, from `https://journals.ametsoc.org/view/journals/clim/31/2/jcli-d-17-0087.1.xml` (Publisher: American Meteorological Society Section: Journal of Climate) doi: 10.1175/JCLI-D-17-0087.1

Becker, T., & Wing, A. A. (2020). Understanding the Extreme Spread in Climate Sensitivity within the Radiative-Convective Equilibrium Model Intercomparison Project. *Journal of Advances in Modeling Earth Systems*, *12*(10), e2020MS002165. Retrieved 2020-11-11, from `https://agupubs.onlinelibrary.wiley.com/doi/abs/10.1029/2020MS002165` (_eprint: https://agupubs.onlinelibrary.wiley.com/doi/pdf/10.1029/2020MS002165) doi: https://doi.org/10.1029/2020MS002165

Ceppi, P., Brient, F., Zelinka, M. D., & Hartmann, D. L. (2017). Cloud feedback mechanisms and their representation in global climate models. *Wiley Inter-*

disciplinary Reviews: Climate Change, *8*(4), e465. Retrieved 2019-07-15, from https://onlinelibrary.wiley.com/doi/abs/10.1002/wcc.465 doi: 10.1002/wcc.465

Ceppi, P., & Gregory, J. M. (2019, October). A refined model for the Earth's global energy balance. *Climate Dynamics*, *53*(7), 4781–4797. Retrieved 2020-12-03, from https://doi.org/10.1007/s00382-019-04825-x doi: 10.1007/s00382-019-04825-x

Flannaghan, T. J., Fueglistaler, S., Held, I. M., Po-Chedley, S., Wyman, B., & Zhao, M. (2014). Tropical temperature trends in Atmospheric General Circulation Model simulations and the impact of uncertainties in observed SSTs. *Journal of Geophysical Research: Atmospheres*, *119*(23), 13,327–13,337. Retrieved 2021-10-12, from https://onlinelibrary.wiley.com/doi/abs/10.1002/2014JD022365 (_eprint: https://onlinelibrary.wiley.com/doi/pdf/10.1002/2014JD022365) doi: 10.1002/2014JD022365

Hansen, J., Sato, M., & Ruedy, R. (1997). Radiative forcing and climate response. *Journal of Geophysical Research: Atmospheres*, *102*(D6), 6831–6864. Retrieved 2019-08-09, from https://agupubs.onlinelibrary.wiley.com/doi/abs/10.1029/96JD03436 doi: 10.1029/96JD03436

Hartmann, D. L. (1994). *Global physical climatology*. San Diego ; London: Academic Press.

Knutti, R., & Rugenstein, M. A. A. (2015, November). Feedbacks, climate sensitivity and the limits of linear models. *Philosophical Transactions of the Royal Society A: Mathematical, Physical and Engineering Sciences*, *373*(2054), 20150146. Retrieved 2019-07-15, from https://royalsocietypublishing.org/doi/full/10.1098/rsta.2015.0146 doi: 10.1098/rsta.2015.0146

Marvel, K., Schmidt, G. A., Miller, R. L., & Nazarenko, L. S. (2016, April). Implications for climate sensitivity from the response to individual forcings. *Nature Climate Change*, *6*(4), 386–389. Retrieved 2021-10-08, from https://www.nature.com/articles/nclimate2888 (Bandiera_abtest: a Cg_type: Nature Research Journals Number: 4 Primary_atype: Research Publisher: Nature Publishing Group Subject_term: Climate and Earth system modelling;Projection and prediction Subject_term_id: climate-and-earth-system-modelling;projection-and-prediction) doi: 10.1038/nclimate2888

Myhre, G., Shindell, D., Bréon, F.-M., Collins, W., Fuglestvedt, J., Huang, J., ... Zhang, H. (2014). *Anthropogenic and Natural Radiative Forcing. In: Climate Change 2013: The Physical Science Basis. Contribution of Working Group I to the Fifth Assessment Report of the Intergovernmental Panel on Climate Change* (Tech. Rep. No. AR5). Retrieved from https://www.ipcc.ch/report/ar5/wg1/ (Publisher: Cambridge University Press)

Pope, V. D., Gallani, M. L., Rowntree, P. R., & Stratton, R. A. (2000, February). The impact of new physical parametrizations in the Hadley Centre climate model: HadAM3. *Climate Dynamics*, *16*(2), 123–146. Retrieved 2021-10-22, from https://doi.org/10.1007/s003820050009 doi: 10.1007/s003820050009

Ramaswamy, V., Boucher, O., Haigh, J., Hauglustaine, D., Haywood, J., Myhre, G., ... Srinivasan, J. (2001). *Radiative Forcing of Climate Change* (Tech. Rep.). IPCC, Geneva, Switzerland. Retrieved from https://www.ipcc.ch/site/assets/uploads/2018/03/TAR-06.pdf

Richardson, T. B., Forster, P. M., Smith, C. J., Maycock, A. C., Wood, T., Andrews, T., ... Watson-Parris, D. (2019). Efficacy of Climate Forcings in PDRMIP Models. *Journal of Geophysical Research: Atmospheres*, *124*(23), 12824–12844. Retrieved 2020-01-17, from https://agupubs.onlinelibrary.wiley.com/doi/abs/10.1029/2019JD030581 doi: 10.1029/2019JD030581

Ringer, M. A., Andrews, T., & Webb, M. J. (2014). Global-mean radiative feedbacks and forcing in atmosphere-only and coupled atmosphere-ocean climate change experiments. *Geophysical Research Letters*, *41*(11), 4035–4042. Retrieved 2021-10-22, from `https://onlinelibrary.wiley.com/doi/abs/10.1002/2014GL060347` (_eprint: https://onlinelibrary.wiley.com/doi/pdf/10.1002/2014GL060347) doi: 10.1002/2014GL060347

Rose, B. E. J., Armour, K. C., Battisti, D. S., Feldl, N., & Koll, D. D. B. (2014). The dependence of transient climate sensitivity and radiative feedbacks on the spatial pattern of ocean heat uptake. *Geophysical Research Letters*, *41*(3), 1071–1078. Retrieved 2021-11-01, from `https://onlinelibrary.wiley.com/doi/abs/10.1002/2013GL058955` (_eprint: https://onlinelibrary.wiley.com/doi/pdf/10.1002/2013GL058955) doi: 10.1002/2013GL058955

Rose, B. E. J., & Rayborn, L. (2016, December). The Effects of Ocean Heat Uptake on Transient Climate Sensitivity. *Current Climate Change Reports*, *2*(4), 190–201. Retrieved 2021-11-01, from `http://link.springer.com/10.1007/s40641-016-0048-4` doi: 10.1007/s40641-016-0048-4

Sherwood, S. C., Bony, S., Boucher, O., Bretherton, C., Forster, P. M., Gregory, J. M., & Stevens, B. (2015, February). Adjustments in the Forcing-Feedback Framework for Understanding Climate Change. *Bulletin of the American Meteorological Society*, *96*(2), 217–228. Retrieved 2020-12-10, from `https://journals.ametsoc.org/view/journals/bams/96/2/bams-d-13-00167.1.xml` (Publisher: American Meteorological Society Section: Bulletin of the American Meteorological Society) doi: 10.1175/BAMS-D-13-00167.1

Shindell, D. T. (2014, April). Inhomogeneous forcing and transient climate sensitivity. *Nature Climate Change*, *4*(4), 274–277. Retrieved 2021-09-10, from `http://www.nature.com/articles/nclimate2136` doi: 10.1038/nclimate2136

Smith, C. J., Kramer, R. J., Myhre, G., Alterskjær, K., Collins, W., Sima, A., ... Forster, P. M. (2020, January). *Effective radiative forcing and adjustments in CMIP6 models* (preprint). Radiation/Atmospheric Modelling/Troposphere/Physics (physical properties and processes). Retrieved 2020-02-05, from `https://www.atmos-chem-phys-discuss.net/acp-2019-1212/` doi: 10.5194/acp-2019-1212

Sobel, A. H. (2002). The ENSO Signal in Tropical Tropospheric Temperature. *JOURNAL OF CLIMATE*, *15*, 5.

Wood, R., & Bretherton, C. S. (2006, December). On the Relationship between Stratiform Low Cloud Cover and Lower-Tropospheric Stability. *Journal of Climate*, *19*(24), 6425–6432. Retrieved 2019-09-16, from `https://journals.ametsoc.org/doi/full/10.1175/JCLI3988.1` doi: 10.1175/JCLI3988.1

Zelinka, M. D., Myers, T. A., McCoy, D. T., Po-Chedley, S., Caldwell, P. M., Ceppi, P., ... Taylor, K. E. (2020). Causes of Higher Climate Sensitivity in CMIP6 Models. *Geophysical Research Letters*, *47*(1), e2019GL085782. Retrieved 2020-05-12, from `https://agupubs.onlinelibrary.wiley.com/doi/abs/10.1029/2019GL085782` (_eprint: https://agupubs.onlinelibrary.wiley.com/doi/pdf/10.1029/2019GL085782) doi: 10.1029/2019GL085782

Zhou, C., Zelinka, M. D., & Klein, S. A. (2016, December). Impact of decadal cloud variations on the Earth's energy budget. *Nature Geoscience*, *9*(12), 871–874. Retrieved 2021-10-12, from `http://www.nature.com/articles/ngeo2828` doi: 10.1038/ngeo2828

Zhou, C., Zelinka, M. D., & Klein, S. A. (2017). Analyzing the dependence of global cloud feedback on the spatial pattern of sea surface temperature change with a Green's function approach. *Journal of Advances in Modeling Earth Systems*, *9*(5), 2174–2189. Retrieved 2021-06-17, from https://agupubs.onlinelibrary.wiley.com/doi/abs/10.1002/2017MS001096 (_eprint: https://agupubs.onlinelibrary.wiley.com/doi/pdf/10.1002/2017MS001096) doi: 10.1002/2017MS001096

Figure 1.

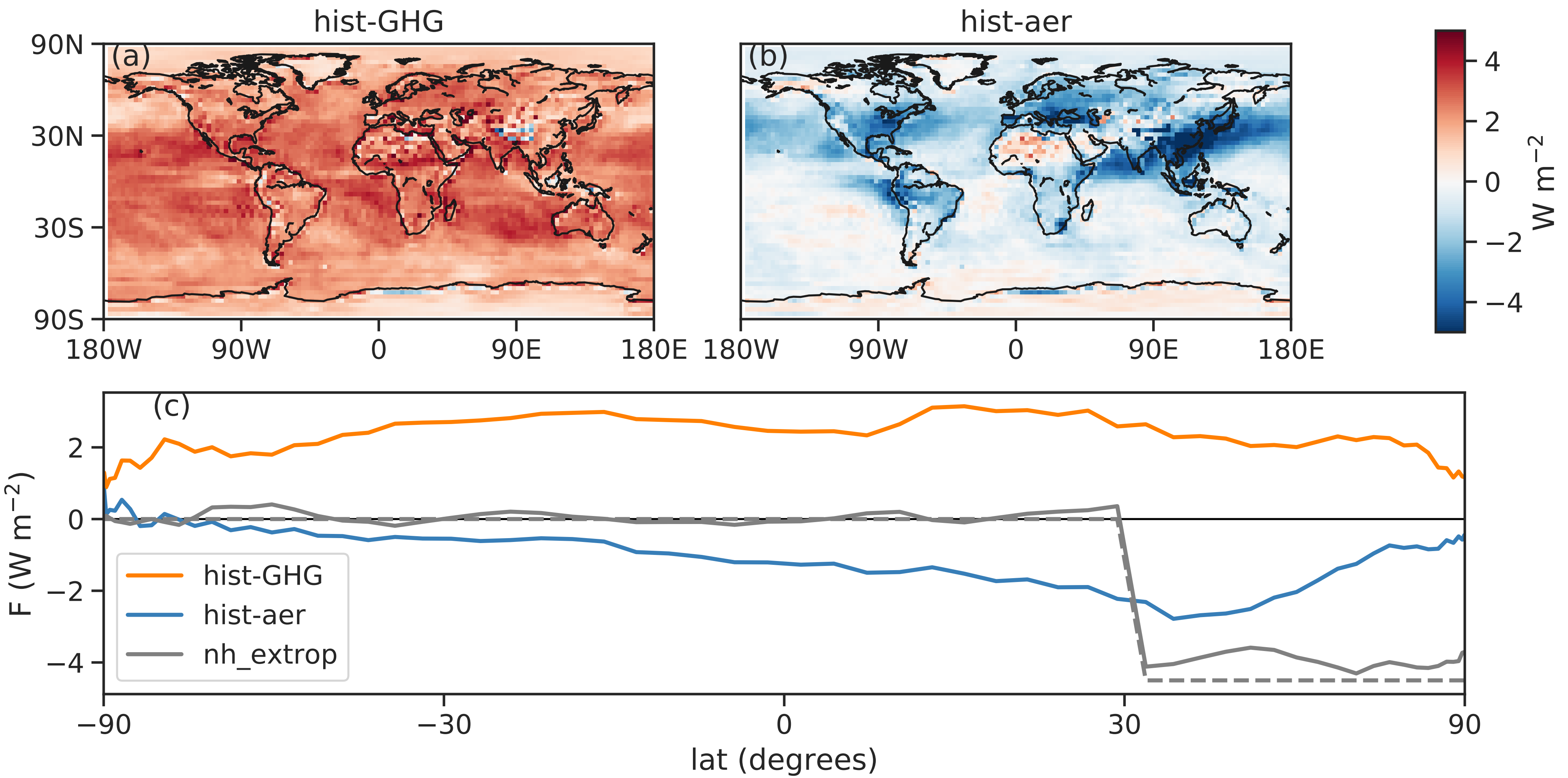
hist-GHG
hist-aer
(a)
(b)
(c)
90N
30N
30S
90S
180W
90W
0
90E
180E
4
2
0
−2
−4
W m^{-2}
F (W m^{-2})
hist-GHG
hist-aer
nh_extrop
−90
−30
0
30
90
lat (degrees)

Figure 2.

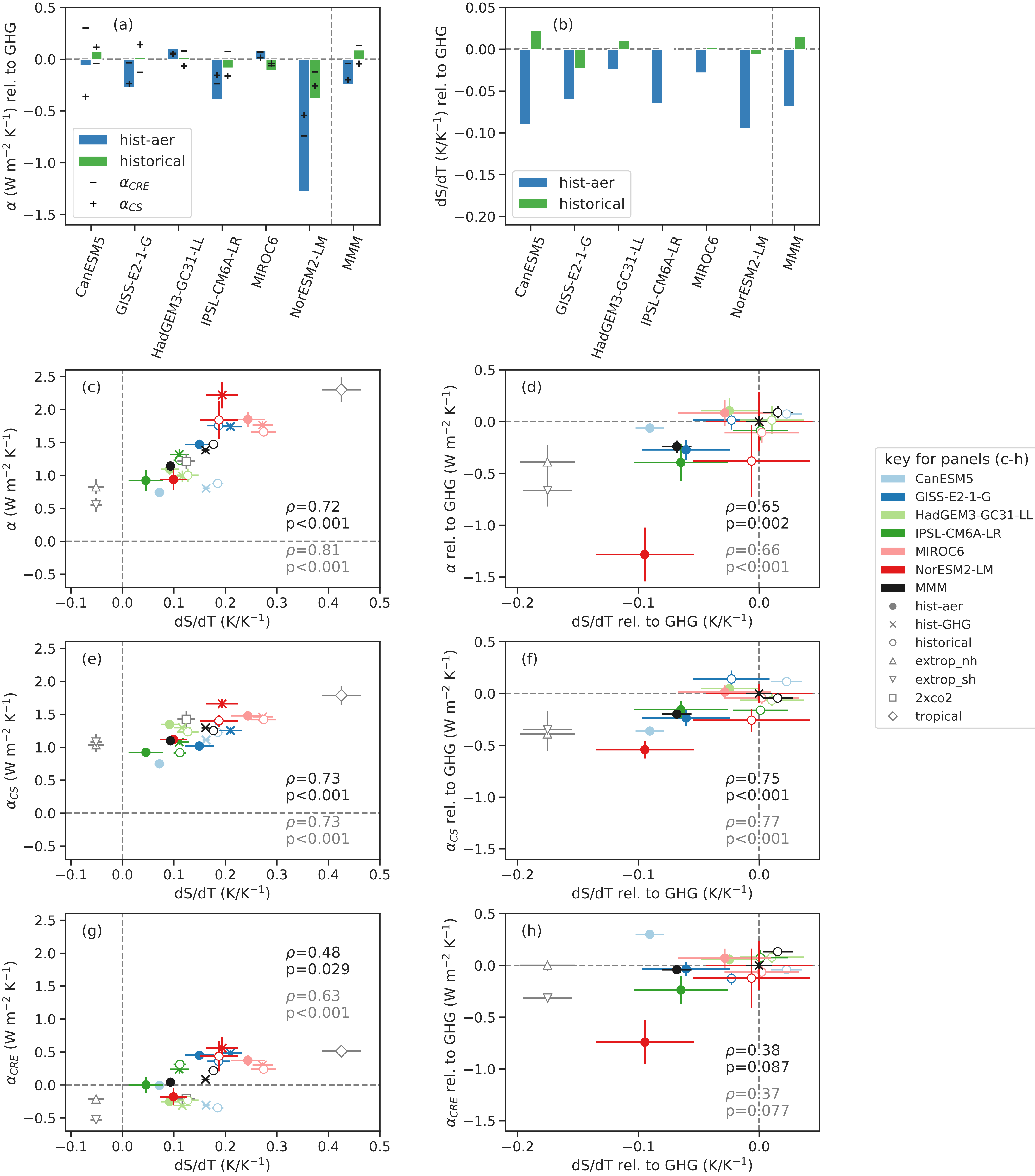

(a)
α (W m^{-2} K^{-1}) rel. to GHG
hist-aer
historical
α_{CRE}
α_{CS}
CanESM5
GISS-E2-1-G
HadGEM3-GC31-LL
IPSL-CM6A-LR
MIROC6
NorESM2-LM
MMM
(b)
dS/dT (K/K^{-1}) rel. to GHG
(c)
α (W m^{-2} K^{-1})
dS/dT (K/K^{-1})
ρ=0.72
p<0.001
ρ=0.81
p<0.001
(d)
α rel. to GHG (W m^{-2} K^{-1})
dS/dT rel. to GHG (K/K^{-1})
ρ=0.65
p=0.002
ρ=0.66
p<0.001
key for panels (c-h)
CanESM5
GISS-E2-1-G
HadGEM3-GC31-LL
IPSL-CM6A-LR
MIROC6
NorESM2-LM
MMM
hist-aer
hist-GHG
historical
extrop_nh
extrop_sh
2xco2
tropical
(e)
α_{CS} (W m^{-2} K^{-1})
ρ=0.73
p<0.001
ρ=0.73
p<0.001
(f)
α_{CS} rel. to GHG (W m^{-2} K^{-1})
ρ=0.75
p<0.001
ρ=0.77
p<0.001
(g)
α_{CRE} (W m^{-2} K^{-1})
ρ=0.48
p=0.029
ρ=0.63
p<0.001
(h)
α_{CRE} rel. to GHG (W m^{-2} K^{-1})
ρ=0.38
p=0.087
ρ=0.37
p=0.077

Figure 3.

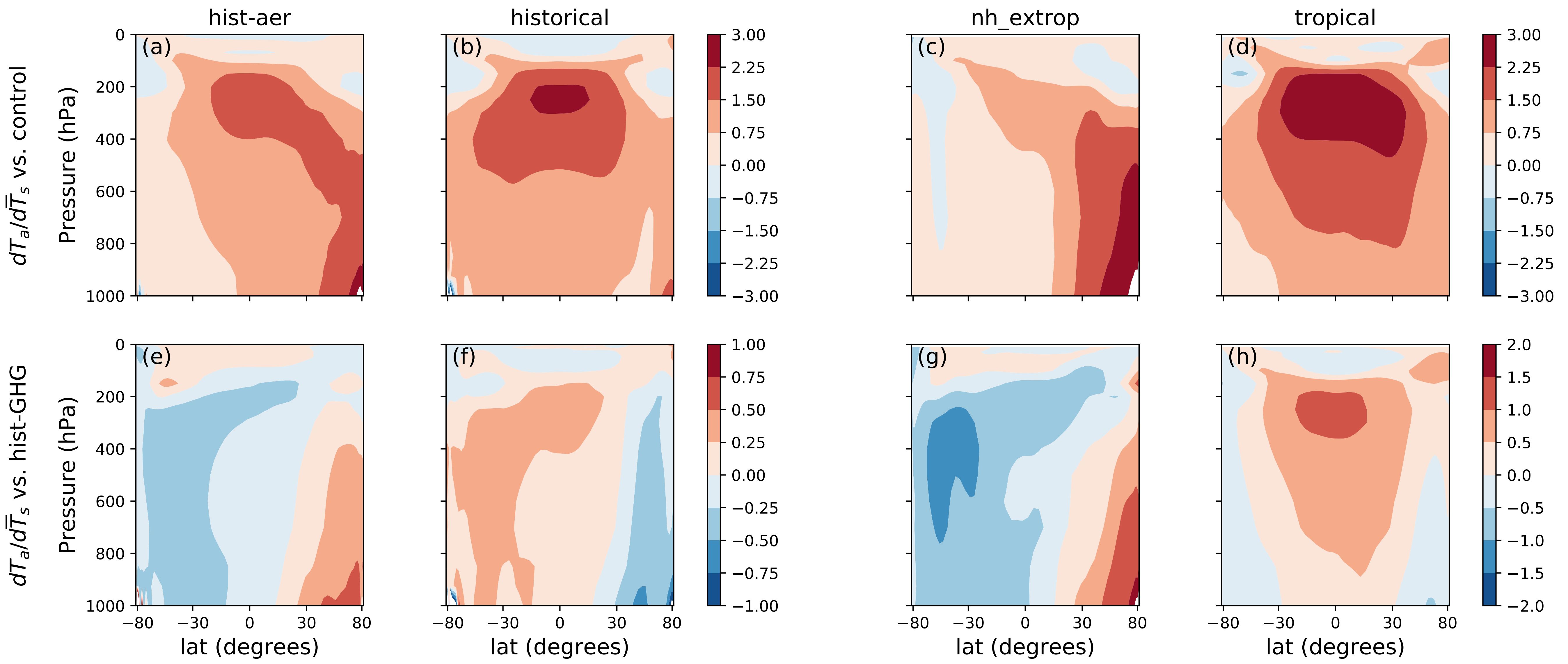

hist-aer
historical
nh_extrop
tropical
(a)
(b)
(c)
(d)
(e)
(f)
(g)
(h)
$dT_a/d\bar{T}_s$ vs. control
$dT_a/d\bar{T}_s$ vs. hist-GHG
Pressure (hPa)
0
200
400
600
800
1000
lat (degrees)
−80
−30
0
30
80
3.00
2.25
1.50
0.75
0.00
−0.75
−1.50
−2.25
−3.00
1.00
0.75
0.50
0.25
0.00
−0.25
−0.50
−0.75
−1.00
2.0
1.5
1.0
0.5
0.0
−0.5
−1.0
−1.5
−2.0

Figure 4.

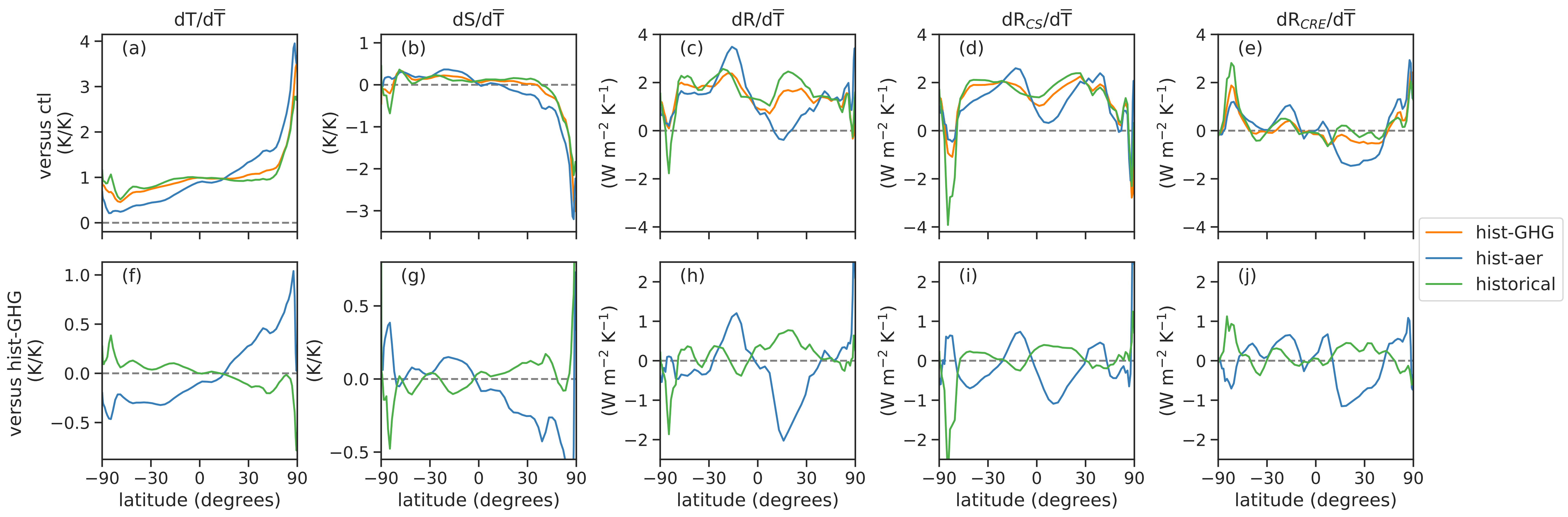
dT/dT̄
dS/dT̄
dR/dT̄
dR_CS/dT̄
dR_CRE/dT̄
versus ctl
(K/K)
versus hist-GHG
(K/K)
(K/K)
(W m^−2 K^−1)
(a)
(b)
(c)
(d)
(e)
(f)
(g)
(h)
(i)
(j)
hist-GHG
hist-aer
historical
latitude (degrees)
−90
−30
0
30
90

Supporting Information for "Interpreting Differences in Radiative Feedbacks from Aerosols Versus Greenhouse Gases"

Pietro Salvi[1], Paulo Ceppi[1], Jonathan M. Gregory[2,3]

[1]Department of Physics & Grantham Institute, Imperial College London, London, UK

[2]National Centre for Atmospheric Science, University of Reading, Reading, UK

[3]Met Office Hadley Centre, Exeter, UK

Contents of this file

1. Tables S1 to S2
2. Figures S1 to S2

Table S1. Experiment names and details for the CMIP6 experiments used in this paper. The "piClim" prefix denotes fixed-SST experiments, while the rest are coupled atmosphere-ocean experiments. piClim-control is an AGCM experiment with SSTs and sea ice climatologies taken from piControl. The fourth column includes three prescribed-SST experiments: piClim-histall, piClim-histGHG and piClim-histaer.

	piClim-control	**hist-GHG** & **hist-aer**	**historical**	**piClim-histxxx**
CanESM5	r1i1p2f1	r[1-10]i1p2f1	r[1-10]i1p2f1	r1i1p2f1
GISS-E2-1-G	r1i1p1f1	r[1-5]i1p1f1	r[1-10]i1p1f1	r1i1p1f1
HadGEM3-GC31-LL	r1i1p1f3	r[1-4]i1p1f3	r[1-5]i1p1f3	r[1-3]i1p1f3
IPSL-CM6A-LR	r1i1p1f1	r[1-10]i1p1f1	r[1-10]i1p1f1	r1i1p1f1
MIROC6	r1i1p1f1	r[1-3]i1p1f1	r[1-10]i1p1f1	r[1-3]i1p1f1
NorESM2-LM	r1i1p1f1	r[1-3]i1p1f1	r[1-3]i1p1f1	r1i1p1f1

Table S2. All-sky radiative feedback parameter (α), CRE (α_{CRE}), and clear-sky radiative feedback parameters (α_{CS}) for each model and the multi-model mean, to 2 d.p. Also shown is the estimated error from variance in the historical variants ($\sigma_{\mathrm{historical}}$).

	hist-aer	**hist-GHG**	**historical**	$\sigma_{\mathrm{historical}}$
CanESM5	0.75	0.80	0.87	0.02
GISS-E2-1-G	1.45	1.69	1.71	0.02
HadGEM3-GC31-LL	1.09	0.98	1.00	0.08
IPSL-CM6A-LR	0.96	1.31	1.22	0.02
MIROC6	1.86	1.78	1.68	0.04
NorESM2-LM	0.95	2.24	1.90	0.04
MMM	1.14	1.37	1.46	0.02

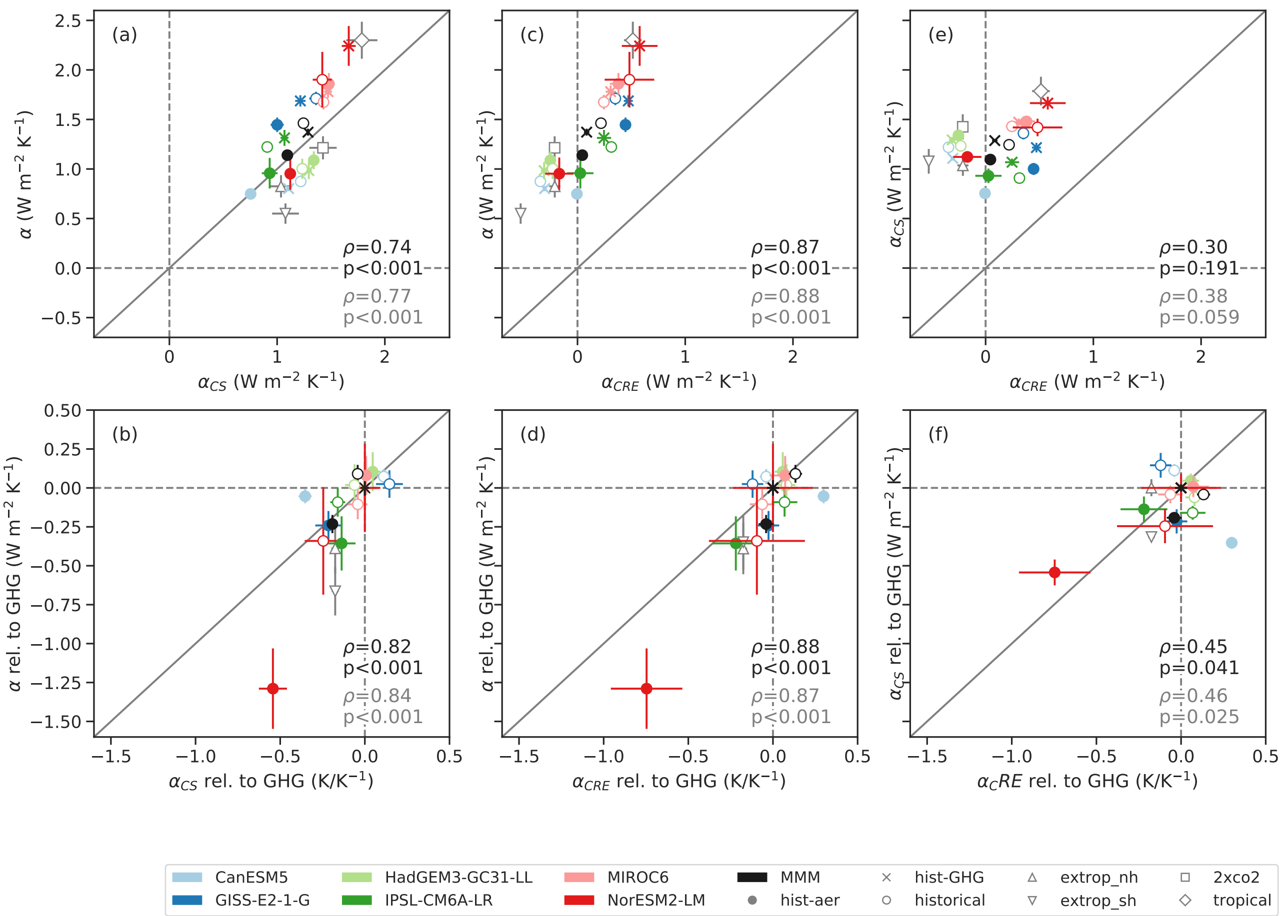

Figure S1. A similar plot as Fig. 2 in the main text, comparing the all-sky radiative feedback parameter (α) to CRE (α_{CRE}) and clear-sky radiative feedback parameters (α_{CS}) for each model and the multi-model mean. Values are shown as absolutes (*top* row) and as the difference from hist-GHG values (*bottom* row). All panels contain a 1:1 line (*solid grey*)

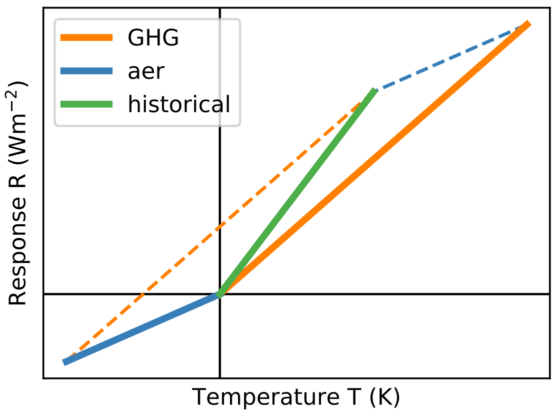

Figure S2. A geometric explanation of why the historical all-forcing feedbacks do not lie between the historical aerosol and historical GHG feedbacks. If the all historical is roughly a linear combination of the historical aerosol (*blue*) and historical GHG (*orange*) results, and the historical aerosol induces a negative temperature change with negative forcing unlike the positive forcing and temperature change from GHGs, then the all historical feedbacks parameter (the gradient of the *green* line) will be more positive than the hist-GHG feedback parameter.

Appendix A Why $\frac{\Delta X_{hist}}{\Delta \overline{T}_{hist}} - \frac{\Delta X_{GHG}}{\Delta \overline{T}_{GHG}}$ anti-correlates well with $\frac{\Delta X_{aer}}{\Delta \overline{T}_{aer}} - \frac{\Delta X_{GHG}}{\Delta \overline{T}_{GHG}}$

We expect that the results from the historical case can be approximated as a sum of hist-GHG and hist-aer cases:

$$\Delta X_{hist} \approx \Delta X_{GHG} + \Delta X_{aer} \tag{A1}$$

$$\Delta \overline{T}_{hist} \approx \Delta \overline{T}_{GHG} + \Delta \overline{T}_{aer} \tag{A2}$$

Given that the global average surface air temperature changes $\Delta \overline{T}$ are, by definition, constants in latitude and longitude, we can relate $\Delta \overline{T}_{GHG}$ and $\Delta \overline{T}_{aer}$ by some function of time a:

$$\Delta \overline{T}_{aer} = a \cdot \Delta \overline{T}_{GHG} \tag{A3}$$

This allows us to rewrite the expression, for the difference between feedbacks in the historical case and the GHG case, in the following way:

$$\begin{aligned}
\frac{\Delta X_{hist}}{\Delta \overline{T}_{hist}} - \frac{\Delta X_{GHG}}{\Delta \overline{T}_{GHG}} &= \frac{\Delta X_{GHG} + \Delta X_{aer}}{\Delta \overline{T}_{GHG} + \Delta \overline{T}_{aer}} - \frac{\Delta X_{GHG}}{\Delta \overline{T}_{GHG}} \\
&= \frac{\Delta X_{GHG}}{\Delta \overline{T}_{GHG} + \Delta \overline{T}_{aer}} + \frac{\Delta X_{aer}}{\Delta \overline{T}_{GHG} + \Delta \overline{T}_{aer}} - \frac{\Delta X_{GHG}}{\Delta \overline{T}_{GHG}} \\
&= \frac{\Delta X_{GHG}}{(a+1) \cdot \Delta \overline{T}_{GHG}} + \frac{\Delta X_{aer}}{(\frac{1}{a}+1) \cdot \Delta \overline{T}_{aer}} - \frac{\Delta X_{GHG}}{\Delta \overline{T}_{GHG}} \\
&= \frac{\Delta X_{GHG}}{(a+1) \cdot \Delta \overline{T}_{GHG}} + \frac{a \cdot \Delta X_{aer}}{(a+1) \cdot \Delta \overline{T}_{aer}} - \frac{\Delta X_{GHG}}{\Delta \overline{T}_{GHG}} \\
&= \frac{a \cdot \Delta X_{aer}}{(a+1)\Delta \overline{T}_{aer}} - \frac{a \cdot \Delta X_{GHG}}{(a+1) \cdot \Delta \overline{T}_{GHG}} \\
&= \frac{a}{(a+1)} \left(\frac{\Delta X_{aer}}{\Delta \overline{T}_{aer}} - \frac{\Delta X_{GHG}}{\Delta \overline{T}_{GHG}} \right)
\end{aligned}$$

We expect that $a < 0$ for all points in time, since we expect aerosol to reduce surface air temperatures where GHGs increase surface air temperatures. We also generally expect that $|a| < 1$ since the historical case gives rising temperatures i.e. the aerosol forcing does not outweigh the GHG forcing. As such, we expect that $\frac{a}{a+1} < 0$ to provide the observed anti-correlation.